DINAME 2017 - Proceedings of the XVII International Symposium on Dynamic Problems of Mechanics
A. T. Fleury, D. A. Rade, P. R. G. Kurka (Editors), ABCM, São Sebastião, SP, Brazil, March 5-10, 2017

Curvature effects on vibrational power flow of smooth bent beams

Paulo Martins[1], **Arcanjo Lenzi**[1]

[1] Universidade Federal de Santa Catarina, R. Lauro Linhares, 1850 - Trindade, Florianópolis - SC, 88070-260, paulo.victor@lva.ufsc.br, arcanjo@lva.ufsc.br

Abstract: This paper discusses an approach to analyze curvature effects on the vibrational powerflow of slender beams. A finite element method (FEM) model was used to calculate transmitted and reflected power via the "propagating wave approach". Previously, the same investigation was addressed with focus on the analytical formulation of curved beams, and an FEM model was programmed using simple two-node straight (Euler-Bernoulli) beam elements. However, the model could simulate in-plane vibrations only, with restrictions to high frequencies (lower than two wavelengths inside the curvature's length). Hence, a new model was proposed, and parametrization of curvatures was updated. A novel method to parametrize the curvature in 3D is discussed using quaternions and Cartesian coordinate systems. Results from the updated FEM model and analytical approach were compared for validation. Moreover, the algorithm performed almost exactly like the analytical model, even at high frequencies, which made it suitable to simulate power flow based on the wave approach. The algorithm allows any type of curve configuration to be tested. Curvature effects for in- and out-of-plane vibrations are shown as well. Finally, this work introduces a tool for designing and optimizing slender pipe structures from the perspective of vibration control.

Keywords: curvature, powerflow, quaternion, FEM, wave approach

INTRODUCTION

The present work mitigates the changes in power flow of vibrational waves while propagating through curved slender beams. The current literature reveals a reasonable amount of work on "smooth bends" and "curves", but the majority only addresses static applications (*e.g.*, structural analysis or civil engineering). Therefore, behavior under a dynamic/vibrational perspective is not well explored for curve configurations.

One can highlight studies that aimed at dynamic behavior, such as the work of Walsh and White (2000), who studied the vibrational power transmission of waves traveling in the same curve's plane. They provided the equations of motion considering different theories: Love's approximations, Flügge's, only rotary inertia, only shear deformation, and Timoshenko (both rotary inertia and shear deformation). They also compared the curved beam's wave numbers with that of a straight beam. The latter was also conducted by Lee *et al.* (2007), who linked wave numbers to power flow by determining analytically how real or imaginary wave numbers can change the power transmission. Lee also reported a "displacement ratio", which is a robust approach to understand how curvatures couple both flexural and longitudinal movement. Wu and Lundberg (1996) also analyzed the vibration in the plane of curvature; they explained the wave propagation approach in a very detailed manner, which consolidated a basis for the present work. They also proposed a non-dimensional set of parameters for analysis that strengthened understanding on the curvature's behavior. Results for constant frequency and curve's parameters were also discussed. For vibrations occurring perpendicular to a curve's plane (out-of-plane vibrations), Wang *et al.* (1980) investigated the natural frequencies for a continuous bent beam and also provided the governing equations for this type of movement. In the numerical approach, Gavric (1992) provided a semi-infinite straight beam element based on its dynamic stiffness, and Davis *et al.* (1972) derived a consistent constant curvature beam element. Both elements are used in finite element analysis.

The next section explains how the curvature will be analyzed, how power from wave constants is obtained, and how the power coefficients are calculated. The third section explains the numerical tool, which is tailored specifically to solve the framework proposed in the second section. The fourth section explains the use of an analytical approach to validate the numerical tool presented in the third section. The fifth section is dedicated to the results and discusses a "map" of curvature effects over power flow. Finally, the last section presents the concluding remarks, as well as some suggestions for future work.

WAVE PROPAGATION APPROACH

Consider an arbitrary wave propagating through a semi-infinite media, which may be longitudinal, torsional or flexural (Figure 1). As this incident wave (superscript I) reaches a curvature (discontinuity), part is reflected (superscript R) and part is transmitted, *i.e.*, passes through and continues (superscript T). The "wave propagation approach" obtains the amplitude constant for each wave type. As this work addresses only the curvature effects, one neglects any type of losses

or damping from the structure.

To obtain the amplitude constants of waves, continuity between both straight and curved interfaces must be guaranteed, *i.e.*, all forces and displacements should be the same at curves ends. Therefore, the formulations of both straight and curved parts are necessary.

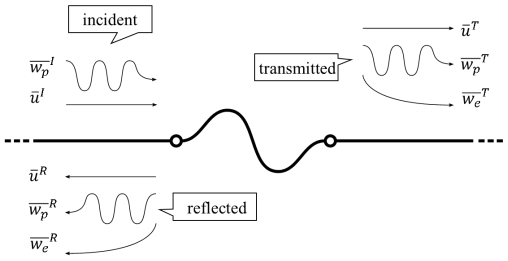

Figure 1 – Diagram of a typical wave approach setup.

First, a straight beam's longitudinal wave is known to have two wave numbers (one for each wave's traveling direction). However, for a single longitudinal wave propagating through a medium in a single direction, one can write

$$u(x,t) = \bar{u}e^{-j(k_u x+\omega t)}, \tag{1}$$

where $\bar{u}$ is the wave constant, $j = \sqrt{-1}$, k_u is the longitudinal wave number, x is the beam's position, ω the angular frequency in rad/s, and t is the time. The other wave solutions can be given in the form

$$\theta_x(x,t) = \bar{\theta}_x e^{-j(k_\theta x+\omega t)}, \qquad w(x,t) = \bar{w}_p e^{-j(k_w x+\omega t)} + \bar{w}_e e^{-(k_w x+j\omega t)}, \tag{2}$$

where $\bar{\theta}_x$ is the propagating torsional constant, $\bar{w}_p$ is the propagating wave constant and $\bar{w}_e$ is the constant of evanescent part. Similarly, the flexural motion on a perpendicular plane will be the same as before if the beam is symmetric. Otherwise, only the wave number k_w is changed.

The wave numbers for a straight beam are

$$k_u = \omega\sqrt{\rho/E}, \quad k_w = \sqrt{\omega^2\rho A/EI_z}, \quad k_v = \sqrt{\omega^2\rho A/EI_y}, \quad k_\theta = \omega\sqrt{\rho/G}, \tag{3}$$

where ρ is the density per length, E is Young's modulus, A is the cross-section's area, I_z and I_y are the area's second moment of inertia on z and y axes, respectively, and G is the shear modulus. Hence, with the configuration shown in Figure 1, one may write the balanced equations for "in-plane" and "out-of-plane" vibration

$$\begin{cases} u_{inlet} = \bar{u}^I e^{-j(k_u x+\omega t)} + \bar{u}^R e^{+j(k_u x-\omega t)}, \\ w_{inlet} = \bar{w}_p^I e^{-j(k_w x+\omega t)} + \bar{w}_p^R e^{+j(k_w x-\omega t)} + \bar{w}_e^R e^{(k_w x-j\omega t)}, \\ u_{outlet} = \bar{u}^T e^{-j(k_u x+\omega t)}, \\ w_{outlet} = \bar{w}_p^T e^{-j(k_w x+\omega t)} + \bar{w}_e^T e^{-(k_w x+j\omega t)}, \\ v_{inlet} = \bar{v}_p^I e^{-j(k_v x+\omega t)} + \bar{v}_p^R e^{+j(k_v x-\omega t)} + \bar{v}_e^R e^{(k_v x-j\omega t)}, \\ \theta_{xinlet} = \bar{\theta}_x{}^I e^{-j(k_\theta x+\omega t)} + \bar{\theta}_x{}^R e^{+j(k_\theta x-\omega t)}, \\ v_{outlet} = \bar{v}_p^T e^{-j(k_v x+\omega t)} + \bar{v}_e^T e^{-(k_v x+j\omega t)}, \\ \theta_{xoutlet} = \bar{\theta}_x{}^T e^{-j(k_\theta x+\omega t)}. \end{cases} \tag{4}$$

Given that $\bar{u}^I$, $\bar{w}_p^I$, $\bar{v}_p^I$ and $\bar{\theta}_x{}^I$ are known, a total of twelve "straight" wave constants need to be determined for the setup. Note that "in-plane" (and subsequently "out-of-plane") is presented in quotation marks because it is referring to a straight beam, whereas a curved section creates a plane for analysis.

Walsh and White (2000) used the propagating wave constants to obtain "in-plane" longitudinal and flexural and "out-of-plane" flexural and torsional powers as follows:

$$W_u = \frac{1}{2}EA\omega k_u\bar{u}^2, \qquad W_v = EI\omega k_v^3\bar{v}^2, \qquad W_w = EI\omega k_w^3\bar{w}^2, \qquad W_\theta = \frac{1}{2}GJ\omega k_\theta\bar{\theta}_x^2, \tag{5}$$

where J is the torsional constant, which can be given by I_z+I_y for a symmetric beam (and rotation axis equals to the centerline).

In the present paper, the concept of "power coefficient" is used to standardize the results as a ratio of transmitted (or reflected) power over the incident power. For example, W_u^T/W_{ip}^I would be a longitudinal transmission coefficient, with $W_{ip}^I = W_u^I + W_w^I$; and W_v^R/W_{op}^I would be an "out-of-plane" reflection coefficient, with $W_{op}^I = W_v^I + W_\theta^I$.

The use of this approach is detailed in the next section, in which the finite element method (FEM) is used to obtain the wave constants and power coefficients.

FINITE ELEMENT SOLUTION

The FEM algorithm must build an arbitrary geometry using beam-like elements so that the user can input mechanical and geometrical properties, such as Young's Modulus (E), shear modulus (G), Poisson's coefficient (ν), density (ρ) and cross-section's dimensions (pipe's diameter and thickness). Moreover, it should simulate the setup with both ends of the geometry as semi-infinite straight beams. Finally, the algorithm should provide the power coefficients as output. The following sub-sections describe the guidelines of how the algorithm was made.

Geometry crafting

Building curvatures in a single plane is somewhat trivial (a single angle and single radius are sufficient to its parametrization), but thinking about three dimensions is much more complicated. One can work with Euler's angles or Rodrigues' rotation, but all of them leave up to three independent angles of rotation and three radii (one for each plane).

To simplify parametrization, inspiration from aviation has been sought, with concepts of an airplane "rolling" (for creating a plane of curve) and "pitching" (for "flying" a curve).

This choice of angles allows a sequence of curved and straight lines to be built using only three known parameters per section: length L, roll angle θ_x, and pitch angle θ_y. The radius of curvature R is obtained as a function of L and θ_y, and it is designated as the "pitching movement". For the "rolling movement" ("airplane" x axis), one has chosen it to occur instantly, before any other "movement" takes part. For example, if the instruction was $L = 10$ mm, $\theta_x = 30^\circ$ and $\theta_y = 90^\circ$, the hypothetical airplane would tilt 30° sideways, and perform a 90° curve with $R \approx 6.37$ mm.

To automate this instruction set, the "geometry builder" algorithm needs a coordinate system in the form of a tensor, which has three columns, each of represents one direction relative to a Cartesian basis:

$$CS = \begin{bmatrix} x_i & y_i & z_i \\ x_j & y_j & z_j \\ x_k & y_k & z_k \end{bmatrix} \tag{6}$$

where i, j and k subscripts represent its global x, y, and z coordinates, respectively. For example, the well-known Cartesian coordinate system ($x = 1i + 0j + 0k$, $y = j$ and $z = k$) could be written as an identity matrix.

Given that every set of instructions to be executed depends on the current (local) coordinate system, quaternion operations can be selected for easy implementation. Kuipers (1999) says that quaternion is a four numbers array, idealized by Irish mathematician William Rowan Hamilton, that is written as:

$$q(\phi, a) = [q_0, q_1, q_2, q_3] = [cos\left(\frac{\phi}{2}\right), sin\left(\frac{\phi}{2}\right)\{a_i, a_j, a_k\}], \tag{7}$$

where ϕ is the desired angle (in *radians*) to rotate the arbitrary object, and $\{a_i, a_j, a_k\}$ is the vector that specifies the direction the rotation will take place over. According to Hamilton (1843), the rotation function can be written in the form

$$CS' = \begin{bmatrix} x_i' & y_i' & z_i' \\ x_j' & y_j' & z_j' \\ x_k' & y_k' & z_k' \end{bmatrix} = RT\left(q(\phi, a), CS\right) = \begin{bmatrix} 1-2q_2^2-2q_3^2 & 2(q_1q_2+q_0q_3) & 2(q_1q_3-q_0q_2) \\ 2(q_1q_2-q_0q_3) & 1-2q_1^2-2q_3^2 & 2(q_2q_3-q_0q_1) \\ 2(q_1q_3+q_0q_2) & 2(q_2q_3-q_0q_1) & 1-2q_1^2-2q_2^2 \end{bmatrix} \begin{bmatrix} x_i & y_i & z_i \\ x_j & y_j & z_j \\ x_k & y_k & z_k \end{bmatrix}, \tag{8}$$

where CS' is the rotated coordinate system, RT is the rotation function, q is the quaternion, and CS is the original coordinate system (before rotation). Therefore, as one needs only to rotate over the local x axis (roll) and y axis (pitch), the "geometry builder" of this work will rely simply on $RT(q(\theta_x, \bar{x}), CS)$ and $RT(q(\theta_y, \bar{y}), CS)$ (being $\bar{x} = \{x_i, x_j, x_k\}$ and $\bar{y} = \{y_i, y_j, y_k\}$) to obtain new coordinate systems. Finally, those rotated coordinate systems will be used by the FEM algorithm to place the elements accordingly.

Finite element formulation

Common Euler-Bernoulli's straight beam elements are commonly used to assemble the global problem's mass and stiffness matrices. The elements of two nodes, and six degrees of freedom per node (three translations and three rotations), can be determined using formulations that are easily found on the Internet.

For completion's sake, the work of Zienkwickz and Taylor (2005) is recommended, from where K_{el} and M_{el} matrices were obtained and given.

Euler's theory of curved beam element for in-plane vibration can be found in the work of Davis *et al.* (1972).

The dynamic stiffness of semi-infinite element and force input (to simulate a wave that is propagating through an infinite media) was taken from Gavric (1992).

The aforementioned formulations can be considered while building a simple FEM algorithm to solve the proposed problem.

Acquisition of wave constants

After assembling the global mass and stiffness matrices and considering harmonic displacement $[u] = [U]e^{-j\omega t}$, and force $[f] = [F]e^{-j\omega t}$, the problem becomes a matter of solving a system of linear equations as

$$\left([K_{gl}] - \omega^2[M_{gl}]\right)[U] = [F]. \tag{9}$$

Therefore, the algorithm performs harmonic analysis, so the focus is to solve the above equation's displacements $[U]$ for each ω, which must not be confused with a wave's constants. To obtain the wave constants from displacements, another system of equations must be built by selecting displacements from known locations and using the straight beam's governing equations (Section 2)

$$\overbrace{\begin{bmatrix} e^{-jk_u s_1} & e^{+jk_u s_1} & 0 \\ e^{-jk_u s_2} & e^{+jk_u s_2} & 0 \\ 0 & 0 & e^{-jk_u s_3} \end{bmatrix}}^{\text{calculated from values of } s \text{ and } \omega} \underbrace{\begin{bmatrix} \bar{u}^I \\ \bar{u}^R \\ \bar{u}^T \end{bmatrix}}_{\text{unknowns}} = \overbrace{\begin{bmatrix} u^1_{inlet} \\ u^2_{inlet} \\ u_{outlet} \end{bmatrix}}^{\text{obtained from FEM solution}} = \begin{bmatrix} U_u(s_1) \\ U_u(s_2) \\ U_u(s_3) \end{bmatrix}, \tag{10}$$

which can be solved by choosing s_1 and s_2 as positions before the curvature, s_3 as a position after the curvature, and $U_u(s)$ as the respective longitudinal displacements onto these positions. Subsequently, $\bar{u}^I$, $\bar{u}^R$ and $\bar{u}^T$ (incident, reflected, and transmitted wave constants, respectively) are solved. The same method can be extended for obtaining the other constants and will be omitted here.

ANALYTICAL VALIDATION

Equations of motion for in-plane and out-of-plane vibrations of curves can be found in the work of Wu and Lundberg (1995) and Wang *et al.* (1980), respectively. The present work shows how to analytically obtain the power coefficients using the governing equations of curves.

In practice, in-plane and out-of-plane motion are coupled, but this coupling is negligible in theory, so the governing equations may be treated separately. Through a balance of forces, Walsh and White (2000), Lee *et al.* (2007) and Wu and Lundberg (1996) give the governing equations for an in-plane vibration. So those will be ommited here for the sake of simplicity.

Considering harmonic displacement $u = \bar{u}e^{-j(ks+\omega t)}$ and $w = \bar{w}e^{-j(ks+\omega t)}$, the equations can be written in a matrix form as

$$\begin{bmatrix} -k^2\left(\frac{EI_z}{R^2} + EA\right) + \omega^2\rho A & jk^3\frac{EI_z}{R} + jk\frac{EA}{R} \\ jk^3\frac{EI_z}{R} + jk\frac{EA}{R} & k^4 EI_z + \frac{EA}{R^2} - \omega^2\rho A \end{bmatrix} \begin{bmatrix} \bar{u} \\ \bar{w} \end{bmatrix} = [0]. \tag{11}$$

Therefore, for a non-trivial solution, the determinant of the matrix should be equal to zero. One can find the characteristic equation that can be solved for the wave number k. This is a sixth order equation that suggests six wave numbers (three pairs of complex conjugates). Hence, the equations of motion for a curved beam are written as

$$u = \sum_{i=1}^{6} \bar{u}_i e^{-j(k_i s+\omega t)}, \qquad w = \sum_{i=1}^{6} \bar{w}_i e^{-j(k_i s+\omega t)}, \tag{12}$$

Yet another simplification can be made before using these equations. From the full matrix form, a "coupling ratio" (referred by Wu and Lundberg as "displacement ratio" and sometimes as "modal component") is expressed as

$$\beta_i = \frac{\bar{u}_i}{\bar{w}_i} = \frac{jk_i^3\frac{EI_z}{R} + jk_i\frac{EA}{R}}{k_i^2\left(\frac{EI_z}{R^2} + EA\right) - \omega^2\rho A}. \tag{13}$$

Thus the equations of motion can be written simply as a function of one displacement type $\bar{w}_i$:

$$u = \sum_{i=1}^{6} \beta_i \bar{w}_i e^{-j(k_i s+\omega t)}, \qquad w = \sum_{i=1}^{6} \bar{w}_i e^{-j(k_i s+\omega t)}, \tag{14}$$

A total of 12 wave constants need to be determined, which comprise six curved wave constants and six straight wave constants (previously introduced). Twelve equations are necessary to assemble a linear system, which can be achieved by equaling displacements and forces from straight and curved parts at both curve's ends

$$u_s^l = u_c^l, \quad w_s^l = w_c^l, \quad \theta_{ys}^l = \theta_{yc}^l, \quad N_s^l = N_c^l, \quad M_{ys}^l = M_{yc}^l, \quad Q_{zs}^l = Q_{zc}^l, \qquad l = inlet, outlet. \tag{15}$$

where l, in this case, represents each end of the curved beam; the subscript s stands for the straight part and c is for the curved part. For the in-plane vibration, one may write

$$\theta_{ys} = -\frac{\partial w_s}{\partial s}, \qquad \theta_{yc} = \frac{u_c}{R} - \frac{\partial w_c}{\partial s}, \tag{16}$$

$$N_s = EA\frac{\partial u_s}{\partial s}, \qquad N_c = EA\left(\frac{\partial u_c}{\partial s} + \frac{w_c}{R}\right), \tag{17}$$

$$M_{y(s,c)} = EI_z\frac{\partial \theta_{y(s,c)}}{\partial s}, \qquad Q_{z(s,c)} = EI_z\frac{\partial^2 \theta_{y(s,c)}}{\partial s^2}. \tag{18}$$

With the previous three sets of equations, the linear system of equations can be solved and the 12 wave constants can be obtained. Hence, four straight propagating wave constants ($\bar{u}^R$, $\bar{u}^T$, $\bar{w}^R$, and $\bar{w}^T$) may be used to calculate the power coefficients via Equation 5, which was introduced previously.

For out-of-plane vibrations, the same procedure follows. By assuming $v = \bar{v}e^{-j(ks+\omega t)}$ and $\theta_x = \bar{\theta}_x e^{-j(ks+\omega t)}$, the governing equation on the matrix form may be written as

$$\begin{bmatrix} -EI_y k^4 - \frac{GJ}{R}k^2 + \rho A\omega^2 & \frac{EI_y}{R}k^2 + \frac{GJ}{R}k^2 \\ \frac{EI_y}{R}k^2 + \frac{GJ}{R}k^2 & -\frac{EI_y}{R^2} - GJk^2 \end{bmatrix} \begin{bmatrix} \bar{v} \\ \bar{\theta}_x \end{bmatrix} = [0]. \tag{19}$$

For a non-trivial solution, the determinant must be null, thereby leading to another characteristic equation for wave number k, which is also of sixth order. The solution leads to three pairs of complex conjugates, which are very close to but not exactly the ones found before. Moreover, coupling occurs between $\bar{v}$ and $\bar{\theta}_x$ in the form

$$\psi_i = \frac{\bar{v}_i}{\bar{\theta}_{xi}} = \frac{\frac{EI_y}{R}k_i^2 + \frac{GJ}{R}k_i^2}{EI_y k_i^4 + \frac{GJ}{R}k_i^2 - \rho A\omega^2}. \tag{20}$$

Thus, by using the same methodology and the following relations

$$\theta_{z(s,c)} = -\frac{\partial v_{(s,c)}}{\partial s}, \tag{21}$$

$$M_{zs} = EI_y\frac{\partial \theta_{zs}}{\partial s}, \quad M_{zc} = -EI_y\left(\frac{\theta_x}{R} - \frac{\partial \theta_{zc}}{\partial s}\right), \tag{22}$$

$$Q_{ys} = EI_y\frac{\partial^2 \theta_{zs}}{\partial s^2}, \quad Q_{yc} = \frac{\partial M_{zc}}{\partial s} - \frac{T_c}{R}, \tag{23}$$

$$T_s = GJ\frac{\partial \theta_{xs}}{\partial s}, \quad T_c = GJ\frac{\partial \theta_{xc}}{\partial s} + \frac{\theta_{zc}}{R}, \tag{24}$$

the linear system of equations may be assembled to obtain the out-of-plane wave constants ($\bar{v}^R$, $\bar{v}^T$, $\bar{\theta}_x^R$, and $\bar{\theta}_x^T$).

Validation results

For an arbitrary curvature of $\Theta_y = 90°$ and $R = 38.2\ mm$ (as depicted in the left of Fig. 2), frequency range of $0 - 10\ kHz$, and prescribing a unitary longitudinal wave, the curves of Figure 2 can be obtained. The right plot shows the differences between numerical and analytical power coefficients for this setup. Colors represent the coefficient's type. Blue is longitudinal transmission W_u^T, yellow is flexural (in-plane) transmission W_w^T, green is longitudinal reflection W_u^R, and wine-red is flexural reflection W_w^R. This Figure 2 indicates a maximum difference of 0.05%.

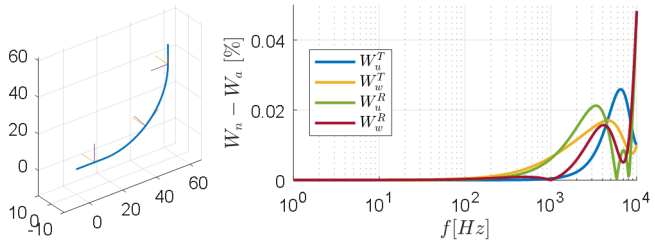

Figure 2 – Differences between numerical and analytical power coefficients, with longitudinal wave input.

For the same geometry, by prescribing a unitary flexural wave, the results of Figure 3 are obtained. The differences are approximately 0.06%, showing an almost exact concordance between numerical and analytical analyses for the in-plane vibration.

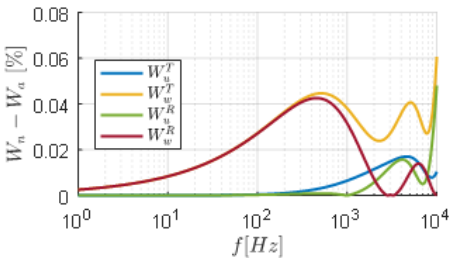

Figure 3 – Differences between numerical and analytical power coefficients, with flexural in-plane wave input.

For a curve with $\Theta_y = 90°$ and $R = 38.2\ mm$, unitary flexural wave perpendicular to the plane of curvature (out-of-plane wave) and torsional wave inputs were tested, and results are shown on Appendix IV.

This approach of plots shows that the difference between numerical and analytical formulations is good to determine how the frequency changes the results. However, this technique provides little information about the overview of differences between the two.

Table 1 – Numerical-analytical differences with IN-PLANE vibration input.

Input	Pitch [°]	W_u^T [%]	W_w^T [%]	W_u^R [%]	W_w^R [%]
$\bar{u}^I$	30	0.018	0.009	0.002	0.007
	60	0.015	0.008	0.004	0.004
	90	0.003	0.002	0.007	0.006
	180	0.002	0.003	0.012	0.008
	270	0.016	0.043	0.089	0.045
	360	0.008	0.006	0.013	0.011
$\bar{w}^I$	30	0.009	0.022	0.007	0.006
	60	0.008	0.014	0.004	0.007
	90	0.002	0.009	0.006	0.005
	180	0.003	0.014	0.007	0.005
	270	0.043	0.114	0.045	0.169
	360	0.006	0.141	0.011	0.144

Table 2 – Numerical-analytical differences with OUT-OF-PLANE vibration input.

Input	Pitch [°]	W_v^T [%]	W_θ^T [%]	W_v^R [%]	W_θ^R [%]
$\bar{v}^I$	30	0.595	0.302	0.110	0.241
	60	0.350	0.206	0.086	0.167
	90	0.970	0.097	0.063	0.804
	180	0.793	0.123	0.075	0.618
	270	0.721	0.080	0.100	0.581
	360	0.698	0.065	0.089	0.619
$\bar{\theta}_x^I$	30	0.802	5.153	0.185	6.012
	60	0.448	2.054	0.098	2.474
	90	0.418	0.353	0.664	1.159
	180	0.435	0.154	0.474	0.796
	270	0.388	0.029	0.441	0.793
	360	0.396	0.040	0.479	0.872

The Tables 1 and 2 show how analytical and numerical approaches differ for all four prescribed wave constants, for cases with $\Theta_y = 30°$, $60°$, $90°$, $180°$, $270°$, and full loop, all with $R = 38.2\ mm$. The worst case scenario was at $\Theta_y = 30°$ for a prescribed torsional wave ($\bar{\theta}_x^I$), with difference of approximately 6% for frequency until 10 kHz. This discrepancy is due to a numerical error generated by the straight elements, because they are not designed to fully represent torsion-to-flexural coupling.

Nevertheless, for the frequency range and application type, the numerical approach is considered validated and good for use.

CURVATURE EFFECTS

This section provides a more general understanding of which curve configurations are prone to let incoming waves pass through (transmit) the bend. This knowledge will allow a sort of "curvature map" of power flow effects. The subsections will address the effects over vibrations occurring in the same curve's plane and then focus on an out-of-plane's effects.

In-plane curvature effects

This analysis involves three parameters analyzed (curvature radius R, angle Θ_y and frequency f), so the transmitted power's coefficient is plotted in a level curve manner (Figure **??**). In this way, for a given radius R, horizontal slices of the plot show transmitted power coefficient per frequency, while each line represents a given angle Θ_y, from 0° to a full loop (360°). By contrast, vertical slices show transmitted power per angles.

Changes in radius simply shift the level curves to the left or right in frequency, as shown for $R = 30$, 100 and 200 mm (Figure 4). Therefore, this method is robust in mapping curvature effects on vibrations.

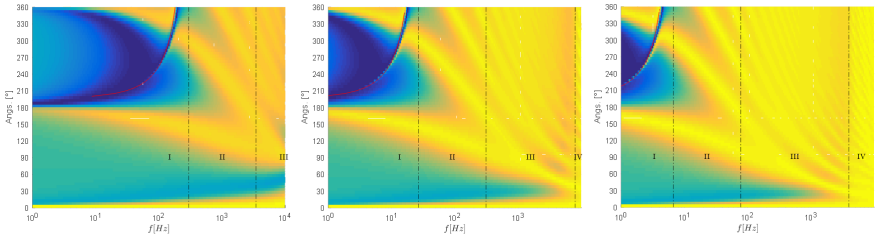

Figure 4 – Power coefficient plots as master curves. left plot shows results for $R = 30$ mm, middle for $R = 100$ mm and right for $R = 200$ mm.

For an arbitrarily chosen radius of 100 mm and prescribing a unitary flexural wave, several repeating regions can be identified over the flexural transmitted power (Figure 5).

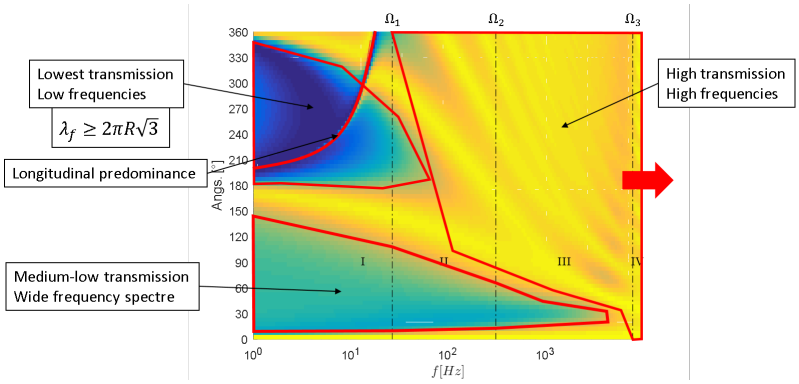

Figure 5 – Power coefficient plots as master curves. Top-left plot shows results for $R = 30$ mm, top-right for $R = 100$ mm and bottom for $R = 200$ mm.

A region of medium to low transmission is present over a wide range of frequency, which occurs for angles $0^\circ < \Theta_y < 150^\circ$. This area is particularly interesting because of its "reflective nature". A high flexural transmission region exists on the plot's top-right portion, which reveals that curvatures are negligible for sufficiently small wave length. Meanwhile, the lowest transmission region can be found at the plot's top-left area (around $180^\circ < \Theta_y < 350^\circ$). This region is heavily dependent on the flexural wave length being greater than $2\pi R\sqrt{3}$, which is the condition for the first cutoff frequency Ω_1 and will be explained immediately after. A red line can be observed from $\Theta \approx 200^\circ$ over a discontinuity, which occurs because of a longitudinal transmission predominance (Figure 6)

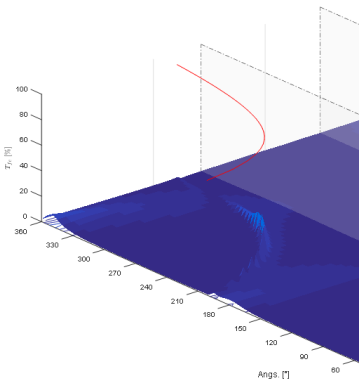

Figure 6 – Power coefficient plots as master curves. Top-left plot shows results for $R = 30$ mm, top-right for $R = 100$ mm and bottom for $R = 200$ mm.

Figure 6 shows only longitudinal transmission W_{tl}^T for the same prescribed flexural wave in 3D. In a region of almost no longitudinal transmission located on the plot's left, a small peak ($\approx 15\%$) of longitudinal transmission can be found.

As observed by Wu and Lundberg (1996), Walsh and White (2000) and Lee *et al.* (2007), those three "cutoff" frequencies are due to a curved beam's wave numbers. Their characteristic behavior involves being real before Ω_1 (or in plot's part I), two becoming complex numbers at II, then turning imaginary at III and finally one of them returning to a real number at IV.

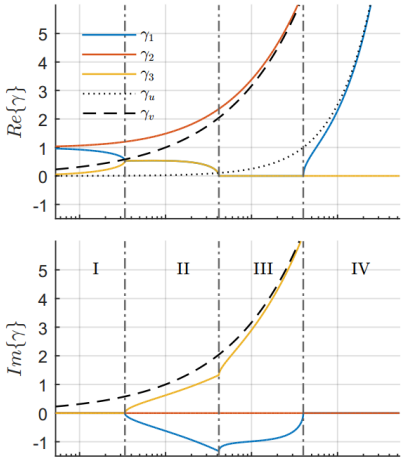

Figure 7 – Wavenumbers for in-plane vibration of a curve.

Figure 7 shows these curved beam's wave numbers (γ_1, γ_2 and γ_3) and compares them with a straight beam wave numbers (γ_u longitudinal and γ_v flexural). Lee *et al.* (2007) also pointed out that Ω_1 and Ω_2 are approximately

$$\Omega_1 \approx \frac{\sqrt{\frac{EI_z}{\rho A}}}{3R^2}, \quad \Omega_2 \approx \frac{\sqrt{\frac{EI_z}{\rho A}}}{R^2}, \tag{25}$$

which leads to $\lambda_f \approx 2\pi R\sqrt{3}$ and πR respectively. This last "cutoff frequency" is called the *ring frequency*, and it is expressed as

$$\Omega_3 = \frac{\sqrt{\frac{I_z}{A}}}{R}, \tag{26}$$

which depends only on geometric properties and occurs at a longitudinal wave length $\lambda_l = 2\pi R$.

One can categorize the first medium-low transmission region as $0^\circ < \Theta_y < 150^\circ$ below Ω_3, the very low transmission region as $180^\circ < \Theta_y < 350^\circ$ until mid-frequency of part II (between Ω_1 and Ω_2), and finally, by exclusion, all other regions as high transmission.

For the longitudinal transmission line, the following formulae can be fit as follows:

$$\Omega_d(\Theta_y) \approx 0.9\Omega_1 - \frac{4.3}{\Theta_y^2 + \sqrt{\Theta_y}}, \tag{27}$$

$$\approx \frac{0.3\sqrt{\frac{EI_z}{\rho A}}}{R^2} - \frac{4.3}{\Theta_y^2 + \sqrt{\Theta_y}}, \tag{28}$$

which depend only on the angle Θ_y and Ω_1, because the discontinuity grows asymptotically to it, as shown in the Figure 5.

Out-of-plane curvature effects

The level curve plots for out-of-plane vibrations are almost the same of those from in-plane vibrations. The main difference is the coupling between flexural out-of-plane and torsional vibrations. However, given that the wave numbers for this case are also very similar to those in the previous case, all discussion about "transmission regions" is valid by analogy (in- and out-of-plane flexural waves, as well as longitudinal and torsional waves, are similar).

A new approach is necessary to investigate 3D effects, so the following setup is proposed: Let there be a simple curve with angle Θ_y (which is the same "curve's angle" Θ_y from before) and length L with an in-plane prescribed flexural wave. This curve will be sliced in the middle ($\Theta_y/2$, therefore $L/2$) and a "rolling" of Θ_x will be applied to the second section.

As this case will be tested for Θ_y from 0° to 360°, Θ_x from 0° to 180°, and frequency f from 0 kHz to 10 kHz, the level curve approach will not suffice because of the extra variable. Therefore, a mean power over frequency is used as a parameter in the form of

$$\bar{W} = \frac{1}{n_f}\sum_{i=1}^{n_f} W. \tag{29}$$

This parameter condenses the results, allowing another "level curve-like" plot. The only disavantage to this approach is the loss of detailed frequency analysis.

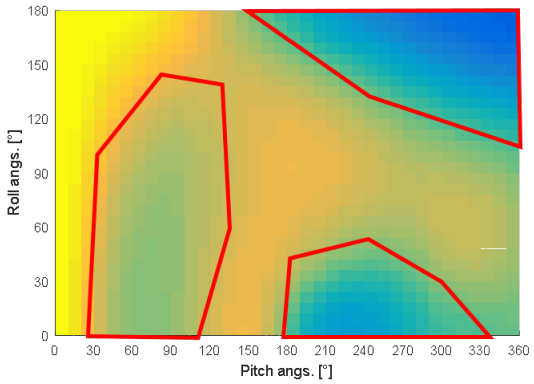

Figure 8 – Condensed mean transmission for out-of-plane flexural vibration acting over a $R = 6\ mm$ curve.

To simplify even further for preliminary analysis, the observed transmitted power is a sum of all transmission coefficients

$$W = W_u^T + W_w^T + W_v^T + W_{\theta x}^T, \tag{30}$$

so that details about a wave's direction are not overwhelming. The results are shown in Figure 8, in which x shows the variation for pitch angles and y axis shows the variation in "rolling angles" (Θ_x), for a $R = 6\ mm$ configuration.

One may immediately detect in Figure 8 some low transmission areas, which are highlighted by red contours: one on the left with curves from 30° to 120° and rolling angles up to about 140° (about 63% of mean power transmission); a small one with low transmission levels (about 34%), with curves from 180° to 330° but rolling angles only going up to 60°; and the lowest transmission's region (reaching below 12%), with curves going from 180° all the way up to a full loop, and rolling angles above 120°.

These regions can be explained by an in-plane level curve map with $R = 6\ mm$, resulting in Figure 9. In- and out-of-plane vibrations are changed in a very similar manner, so one can easily understand why regions above 180° are prone to low transmission levels, given that a small radius will increase the cutoff frequencies, especially the first ($\Omega_1 \approx \sqrt{EI_z/\rho A}/3R^2$).

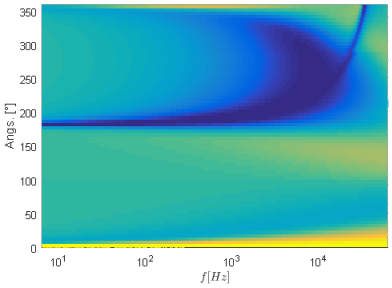

Figure 9 – Power coefficients for a flexural out-of-plane vibration acting over a single $R = 6\ mm$ curve (without the "rolling aspect").

Thus, for a small radius, the best configuration possible is a series of $\Theta_x = 180°$ curves aligned in the same plane.

As the radius increases (now $R = 50\ mm$), the low transmission regions for pitch angles $\Theta_y > 180°$ vanishes, as illustrated in Figure 10.

This phenomenon is due to the low cutoff frequencies, which result from the high transmission region discussed in the previous section. Hence, for 50 mm radius, one should focus on the "medium-to-low transmission" region, with curve angle Θ_y from 20° to 120° and rolling angles higher than 95°.

When the radius is increased even further, the tendency is to obtain more transmission overall. However, starting from $R = 100\ mm$, low power transmission starts to concentrate between $30° < \Theta_y < 60°$ and high rolling angles.

In general, from a vibration's perspective, best case scenario is when the structure have a succession of 50° curves, aligned in the same plane. Evidently, for more complex structures, the curve's radius should be considered to yield better results.

CONCLUSIONS

The present work investigated the changes in power flow of vibrational waves, while propagating through smooth bent slender beams. This paper presented the wave propagation approach, as well as the standardization of results using power

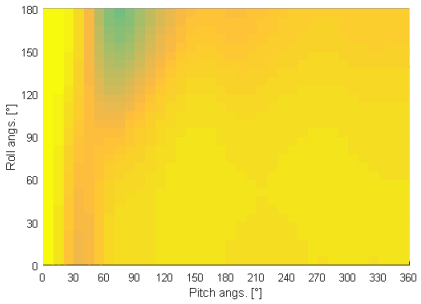

Figure 10 – Condensed mean transmission for out-of-plane flexural vibration acting over a $R = 50\ mm$ curve.

coefficients.

Subsequently, an FEM program was constructed to simulate the proposed approach. The used finite elements were shown, and the power coefficients were obtained through this numerical tool. Analytical validation was carried out, with all formulations for both in-plane and out-of-plane vibrations. Differences between the two were discussed.

With the validated FEM tool, the effects of in-plane and out-of-plane vibrations were discussed in detail. Moreover, different setups for obtaining results from each case were proposed. First, longitudinal and torsional waves do not transmit meaningful vibrational power through curves, except for curve angles nearing 0° and for one "discontinuity line" given by $\Omega_d(\Theta_y) \approx 0.9\Omega_1 - 4.3/(\Theta_y^2 + \sqrt{\Theta_y})$.

Both in- and out-of-plane vibrations are similarly changed when their paths have a smooth bend. Longitudinal waves are analogous to torsional ones, and flexural waves on the same plane of a curve are analogous to the plane perpendicular to the curve.

For the effects of in-plane vibration, three major regions were identified: medium-to-low transmission/wide frequency range, very low frequency/low frequency range and high transmission.

Finally, for sequential out-of-plane curves, the radius plays a huge influence over overall transmitted power. If the cutoff frequencies are sufficiently high, two important low-transmission regions exist for curve angles above 180°. Otherwise, the previously mentioned medium-to-low region is highlighted, showing that the lowest transmission values are between 30° and 120° curves.

This study aimed to enlighten the curvature effects on vibrations, for the benefit of engineers and designers to ease the conception of new products that use curved slender structures.

REFERENCES

Davis, R.; Henshell, R. D.; Warburton, G. B., 1972, "Constant curvature beam finite elements for in-plane vibration", Journal of Sound and Vibration, Elsevier, v. 25, n. 4, p. 561–576.

Gavric, L., 1992, "Power-flow analysis using infinite beam elements", Le Journal de Physique IV, EDP Sciences, v. 2, n. C1, p. C1–511.

Graff, K. F., 1970, "Elastic wave propagation in a curved sonic transmission line", Sonics and Ultrasonics, IEEE Transactions on, IEEE, v. 17, n. 1, p. 1–6.

Hamilton, W. R., 1843, "On quaternions, or on a new system of imaginaries in algebra", Philosophical Magazine, Edited by David R. Wilkins in 2000, Dublin.

Huang, D.; Redekop, D.; Xu, B., 1997, "Natural frequencies and mode shapes of curved pipes". Computers & structures, Elsevier, v. 63, n. 3, p. 465–473.

Kang, B.; Riedel, C. H.; Tan, C. A., 2003, "Free vibration analysis of planar curved beams by wave propagation". Journal of Sound and Vibration, Elsevier, v. 260, n. 1, p. 19–44.

Kuipers, J. B., 1999, "Quaternions and rotation sequences". Princeton Univeristy Press, ISBN 0-691-10298-8

Lee, S. K.; Mace, B. R.; Brennan, M. J., 2007, "Wave propagation, reflection and transmission in curved beams". Journal of Sound and Vibration, Elsevier, v. 306, p. 636–656.

Walsh, S. J.; White, R. G., 2000, "Vibrational power transmission in curved beams", Journal of Sound and Vibration, Elsevier, v. 233, n. 3, p. 455–488.

Wang, T. M.; Nettleton, R. H.; Keita, B., 1980, "Natural Frequencies for Out-of-Plane Vibrations of Continuous Curved Beams", Journal of Sound and Vibration, Elsevier, v. 68, n. 3, pp. 427-436.

Wu, C. M.; Lundberg, B., 1996, "Reflection and transmission of the energy of harmonic elastic waves in a bent bar". Journal of Sound and Vibration, Elsevier, v. 190, n. 4, p. 645–659.

RESPONSIBILITY NOTICE

The author is the only one responsible for the material included in this paper.